Development of innovative therapeutic strategies for osteoarthritis: exploring thermosensitive hydrogels, hiPSC-derived cells and cell-products, and novel drugs in preclinical models

Sayedipour, S.S.

Chapter 2

Poloxamer-based thermosensitive injectable hydrogels containing a self-assembling peptide for *in situ* gelation

S.Sana Sayedipour[1,4], Timo Schomann[1,2], Sanne M. van de Looij[3] , Somayeh Rezaie[1], Yolande F.M. Ramos[4], Tina Vermonden[3], Louise van der Weerd [5], Ingrid Meulenbelt[4]*, and Luis J. Cruz[1]

[1], Department of Radiology, Leiden University Medical Center, 2333 ZA Leiden, the Netherlands

[2], Department of Vascular Surgery, Leiden University Medical Center, 2333 ZA Leiden, the Netherlands

[3],Department of Pharmaceutical Sciences, Utrecht Institute for Pharmaceutical Sciences (UIPS), Utrecht University, 3508 TB Utrecht, the Netherlands

[4], Section Molecular Epidemiology, Department of Biomedical Data Sciences, Leiden University Medical Center, LUMC Postzone S-05-P, P.O. Box 9600, 2300 RC Leiden, the Netherlands

[5],Departments of Radiology & Human Genetics, Leiden University Medical Center, 2333 ZA Leiden, the Netherlands

*Corresponding author

Published in:

Computational and Structural Biotechnology Journal. 2025 Sep 29.

https://doi.org/10.1016/j.csbj.2025.09.034

Abstract

This study presents the development and characterization of a novel thermosensitive injectable hydrogel designed to enhance the biomechanical properties of poloxamer 407 (P407) through the incorporation of a self-assembling peptide. The primary objective was to engineer a formulation that rapidly gels following intra-articular (i.a.) injection, exhibits improved mechanical strength, and enables sustained release of embedded therapeutic cargo.

Gelation time assays demonstrated that the P407-peptide formulation solidified more quickly than P407 alone at equivalent concentrations. Rheological analysis revealed a 1.5 kPa increase in storage modulus in the hybrid hydrogel, confirming improved mechanical integrity. *In vitro* biocompatibility was assessed using human chondrocyte cell line, with MTS assays and LIVE/DEAD staining indicating no cytotoxicity across tested concentrations.

To evaluate *in vivo* applicability, a near-infrared fluorescent (NIRF) dye was incorporated into the hydrogel and injected intra-articularly into an osteoarthritis (OA) mouse model. The labeled formulation allowed for successful tracking and demonstrated localized gelation, supporting its suitability for site-specific, sustained delivery.

Overall, the P407-peptide hydrogel offers a promising platform for i.a. therapeutic applications, combining injectability, rapid thermoresponsive gelation, mechanical reinforcement, and controlled release behavior, making it well-suited for regenerative medicine and OA treatment.

Keywords: Thermosensitive hydrogel | Poloxamer | Self-assembling peptide | *In situ* gelation | Osteoarthritis

1. Introduction

Injectable hydrogels have gained significant attention as drug delivery systems due to their tunable physical properties, minimally invasive administration, and ability to provide sustained release of therapeutics at the target site (1-4). Such properties make thermosensitive hydrogels particularly suitable for intra-articular (i.a.) administration of osteoarthritis (OA) treatments, where encapsulation of therapeutic cells or drugs within the hydrogel matrix enables targeted delivery directly into the joint space (5). In particular, thermosensitive hydrogels are attractive drug delivery systems, remaining liquid at lower temperatures during injection and rapidly forming a gel at physiological temperatures. This temperature-triggered transition enables localized, sustained release of therapeutics, reducing systemic toxicity and minimizing the frequency of administration (6, 7). Among them, Poloxamer 407 (P407) has been widely studied as a result of its unique thermo-reversible gelation properties, low toxicity and sustained drug release characteristics. P407 is a triblock copolymer with a center block of hydrophobic polypropylene oxide (PPO) between two hydrophilic polyethyleneoxide (PEO) lateral chains (8-10). Upon dissolution in water, P407 molecules self-assemble into micelles with a hydrophobic polypropylene oxide (PPO) core and a hydrophilic polyethylene oxide (PEO) shell. When the polymer is sufficiently concentrated and the temperature rises beyond the critical gelation temperature (CGT), these micelles organize into a firm network, leading to the formation of a semi-solid gel depot (11). Despite the multiple benefits of P407, proper application of this gel as carrier of drugs remains problematic due to its rapid dissolution in aqueous media (12, 13) whereas the low mechanical strength precludes its use as a biomimetic hydrogel mimicking extracellular matrix (12, 13). Although higher polymer concentrations can improve gel firmness and delay dissolution, these higher concentrations also result in elevated viscosity at room temperature, causing handling difficulties such as needle clogging during injection (14, 15). Various strategies have been explored to modulate the sol–gel transition temperature ($T_{sol–gel}$) and enhance hydrogel performance to overcome the limitations of P407, including the incorporation of pharmaceutically active ingredients, salts, excipients, and functional biomolecules into P407 formulations (16, 17). Among these approaches, the incorporation of self-assembling peptides has emerged as a particularly effective strategy to improve the structural integrity and functional properties of P407-based hydrogels (18). These peptides can physically interpenetrate or chemically interact with the hydrogel network, improving cargo affinity, inhibiting burst release, and prolonging drug release, thereby making the system more suitable for controlled delivery applications (19). We previously showed that one such peptide, Palmitoyl-WKGNNQQNYQQ, that combines a β-sheet-forming amyloidogenic sequence (KNNQQNYQQ, originally derived from the yeast prion protein Sup35), with an N-terminal palmitoyl group particularly promoted hydrophobic interactions. Moreover, the dual design enabled spontaneous assembly into nanofibers capable of stabilizing polymeric hydrogels (20).

In this study, we set out to test whether incorporating the amphiphilic self-assembling peptide Palmitoyl-WKGNNQQNYQQ into P407 could reinforcing the hydrogel, increase its stability in aqueous solution, and preserving its thermosensitive behavior. Features that could particularly enhance its suitability for preclinical intra-articular applications. For this purpose, we incorporated the near-infrared fluorescent (NIRF) dye IR780 into the hydrogel and administered it via i.a. injection into mice knee joint.

2. Materials and methods

2.1. Materials and reagents

Commercial P407 (MW= 12,600 Da) and phosphate-buffered saline (PBS) were produced by Fresenius Kabi GmbH (Graz, Austria). Dulbecco's phosphate-buffered saline (DPBS), Dulbecco's modified eagles' medium (DMEM, high glucose, with Glutamax^{TM}), fetal bovine serum (FBS), penicillin, and streptomycin were purchased from Life Technologies (Breda, the Netherlands). 3-(4,5-Dimethylthiazol-2-yl)-5-(3-carboxymethoxyphenyl)-2-(4-sulfophe-nyl)-2H- Gels 2022, 8, 44 11 of 16 tetrazolium (MTS, Promega, Madison, WI, USA) and a calcein-AM/ethidium homodimer-1 LIVE/DEAD® assay kit (Invitrogen) were obtained from Carlsbad, CA, USA

2.2. Self-assembling Peptide

Self-assembling peptide with sequence Palmitoyl-WKGNNQQNYQQ, designed by Dr. Luis J. Cruz (Department of Radiology, Leiden University Medical Center, Leiden, the Netherlands) and was synthesized using solid-phase peptide synthesis (SPPS) employing the Fmoc strategy (21) and provided by GL Biochem Ltd. (Minhang, Shanghai, China).

2.3. P407-peptide hydrogel preparation and characterization

2.3.1. P407-peptide hydrogel preparation

P407-peptide composite hydrogel was prepared using the 'cold' method (22). To prepare 30% hydrogel (w/v), 3 gr of poloxamer powder and 100 mg of peptide were gently dissolved in 10 mL of sterilized ultrapure water. The mixture was then stirred at 4 °C overnight to ensure that all the powder dissolved completely, resulting in a clear solution.

2.3.2. Time-to-gelation assay

The gelation behavior of P407 and P407–peptide hydrogels was evaluated using the tube inversion method. Different concentrations of P407 (10, 15, 20, 25, and 30%) were prepared. Based on these 25% P407 and 30% P407 was selected for further experiments. To investigate the effect of increasing peptide concentration on the P407 formulation, various peptide concentrations (1, 2, 3, 4, 5, and 7.5%) were incorporated into the selected solution. For each formulation, 1 mL of hydrogel was transferred into a test tube and incubated in a water bath at either room temperature (RT, 25 °C) or 37 °C. The sol–gel transition temperature was defined as the point at which the solution no longer flowed upon tube inversion, indicating gel formation. Each measurement was performed in triplicate.

2.3.3. Injectability test of Hydrogels

Injectability of selected thermosensitive hydrogel solutions were qualitatively evaluated immediately after their synthesis. Flowability of each solution was measured using syringes with different needle gauge size 18G × 1 1/2 in. (1.2 ×40 mm), 23G × 1 in. (0.6 ×25 mm), 25G ×1/2 in. (0.5 × 16 mm), 30G × 1/2 in (0.3 × 13 mm) at RT and 37 °C. The observations for each hydrogel sol mixture were rated comparatively.

2.3.4. Rheological characterisation

The rheological properties of 25% P407 and 25% P407 containing 1% (w/v) self-assembling peptide were evaluated using a Discovery HR-2 Rheometer (TA Instruments, Etten-Leur, The Netherlands) equipped with a Peltier plate for precise temperature control and a solvent trap to minimize sample evaporation. Both samples were measured using a 20 mm diameter aluminium plate-plate geometry and an initial gap of 300µm. Hydrogel formulations were prepared, and 100 µL sample were deposited under the geometry for measurements. Data were processed with TRIOS Software version 5.1. The appropriate strain for all samples was determined by formation of the hydrogel formulations at 37 °C for 30 min, followed by an oscillation amplitude with increasing strain from 0.01% to 100% at a frequency of 1 Hz. Gelation kinetics were then assessed by measuring the storage (G') and loss (G'') moduli during a temperature ramp ranging from 4 °C to 37 °C at a rate of 1.0°C.min^{-1}, using a frequency of 1 Hz and a strain of 0.1%. Next, the samples were kept at 37 °C for 15 min, before cooling down to 4°C at a rate of 1.0°C.min^{-1}. Each measurement was performed in triplicate.

2.3.4. Morphology of P407, self-assembled peptide network and P407-peptide hydrogels by scanning electron microscopy (SEM)

A 25% (w/v) solution of P407 and an equivalent concentration of 25% P407 containing 1% (w/v) self-assembling peptide were frozen at −80 °C and subsequently lyophilized to examine hydrogel morphology. After freeze-drying, small pieces of each sample were cut, mounted on aluminum stubs, and sputter-coated with a platinum layer using a Cressington 208HR sputter coater (Cressington, Watford, UK). The surface structure was imaged by NanoSEM 450 scanning electron microscope (FEI, Tokyo, Japan). Pore size was quantified from SEM micrographs using Fiji/ImageJ (version 1.54p). For each condition, 3 samples and ≥5 fields of view per sample were analyzed.

2.3.5. Dynamic light scattering (DLS) measurements

Samples with different concentrations of P407 and P407-peptide (1, 2, 3, 4, 5, 7.5 and 10%) were prepared in MilliQ H_2O (Merck-Millipore, Burlington, MA, USA) to study the properties of P407 micelles. Approximately 800 mL of the samples were then transferred to cuvettes for measurement using a Zetasizer (Nano ZS, Malvern Ltd., Malvern, UK). Measurements were performed at 20 °C, with

three independent acquisitions per sample. The hydrodynamic diameter and polydispersity index (PDI) were recorded from the intensity distribution.

2.3.6. P407 and P407-peptide hydrogel degradation

The release kinetics of P407-peptide hydrogel were assessed using the direct release method, with NIRF dye IR780 as the loaded cargo (13, 23). In brief, 50 ng of IR780 was mixed with 1 mL of 25.0% (w/v) P407 and P407-peptide hydrogels in 15 mL tubes at 4°C. The tubes were then incubated at 37°C for 5 min to allow the formation of a stable gel. After gel formation, 4 mL of pre-warmed PBS was gently added on top of the gel layer, and the tubes were placed in a shaking water bath at 37 °C and 30 rpm. At specific time points until the hole hydrogel in both sample degrades (1, 2, 4, 8, 12, 24, 48, 72, 96, 120, 144, 168, 192, and 216 h), 1 mL of supernatant was collected from each tube, and the volume was replaced with fresh PBS pre-warmed to 37 °C. The released IR780 was then quantified using SpectraMax® iD3 Multi-Mode Microplate Readers (Marshall Scientific, Hampton, NH, USA). Additionally, the degradation of the hydrogels was evaluated. Briefly, 1 mL of hydrogel was placed in 15 mL falcon tubes and incubated at 37 °C for gel formation. The initial weight of the tube with hydrogel was recorded as 100% of the gel weight. Following this, 4 mL of pre-warmed PBS was added on top of the hydrogel. At predetermined time points corresponding to those in the release measurement, the entire volume was removed, and the weight was measured to calculate the amount of hydrogel degradation.

2.4. *In vitro* experiment

2.4.1. Cell culture

The human chondrocyte cell line C28/I2 was cultured in 75 cm2 flasks containing a 1:1 mixture of DMEM and F12 medium with 10 % (v/v) FBS at 37 °C and 5% CO_2. The medium was refreshed every 48 h. Once the cells reached 80-90 % confluence, they were subcultured for experiments.

2.4.2. Cell metabolic assay (MTS)

The effect of P407 and peptide on C28/I2 cells was evaluated using the MTS colorimetric method (24). Cells were seeded in a 96-well plate at a density of 5×10^3 cells per well. Hydrogels of 25% P407 or 25% P407- peptide were prepared in DMEM and added to the wells for 24, 48, and 72 h. Untreated cells served as negative control, while cells treated with 50 % DMSO served as positive, cytotoxicity control. After each time point, the old medium was carefully removed and replaced with 100 µL of fresh medium plus 20 µL of [3-(4,5-dimethylthiazol- 2-yl)-5-(3-carboxymethoxyphenyl)-2-(4-sulfophenyl)-2H-tetrazolium (MTS) in each well. After 1 h of incubation at 37 °C, the optical density was measured using a spectrophotometer at λ_{ex} 590 nm. Each measurement was performed in triplicate.

2.4.3. Cell viability (LIVE/DEAD® assay)

The effect of 25% P407-peptide hydrogels on the viability of C28/I2 cells was evaluated using a LIVE/DEAD® assay at 1, 3, and 7 days after culture. A total of 2×10^4 C28/I2 cells/well were seeded on top of the 25% P407-peptide hydrogels in a 48-well plate and incubated for 1, 3 and 7 days. After removing the supernatant, an aliquot of the assay solution containing 4 µM EthD-1 (ethidium homodimer-1) and 2 M calcein AM was added to the cells. Following a 25 min incubation, the samples were observed using an Andor Dragonfly 200 spinning disc confocal microscope (Andor Technology, Belfast, UK) with excitation filters of 450–49 nm (green, Calcein AM) and 510–560 nm (red, EthE-1). Living cells were visualized as green and dead cells were visualized as red. Quantification of LIVE/DEAD staining was performed in Fiji/ImageJ (version 1.54p). For each condition, three independent, non-overlapping fields were analyzed. Images were split into green (live) and red (dead) channels, background was removed, and a single threshold per channel was defined on representative images and then applied identically to all images. Live and dead cells were counted in each frame, and the data were analyzed.

2.5. *In vivo* experiment

2.5.1. Animal model

To evaluate the concept of our thermosensitive, injectable P407-peptide hydrogel and its degradation and steady release of near-infrared fluorescent (NIRF) dye IR780, we performed *in vivo* i.a. injections in mice knee joints. Notable is that these injections of P407-peptide hydrogel were part of a larger preclinical mouse study in which destabilization of the medial meniscus (DMM) was used to induce osteoarthritis related damage to the cartilage. For the current manuscript a total of eighteen (3 groups, each 6 mice) 12 weeks-old male C57BL/6J mice were used from Charles River Laboratories (Charles River, Chatillon-sur-Chalaronne, France). The animal procedures were all conducted at the Leiden University Medical Center and were approved by the Animal Welfare Committee (IvD) under number AVD1160020171405 - PE.18.101.005. All mice were housed in groups in polypropylene cages on a 12-hour light/dark cycle with unrestricted access to standard mouse food and water. Surgical destabilization of the medial meniscus was performed on the right knee joint as described before (25). Thee weeks after the surgery, DMM mice were randomly divided into 3 groups, receiving 6 µL of either saline plus 50 ng of IR780, P407 loaded with IR780, or P407-peptide loaded via i.a. injection by 30G needle. These mice were sacrificed 34 days after the injections, and their limbs were and studied by means of fluorescence imaging for signs of scaffold degradation.

2.5.2. *In vivo* imaging

To evaluate the degradation and stability of the thermosensitive hydrogel mixed with IR780, NIRF imaging was assessed using the Pearl Impulse Imaging System (Li-Cor, Lincoln, NE, USA). Mice were anesthetized using isoflurane (4–5% induction, 1–2% maintenance) and imaged at 1, 7, 14, 21, 28, and 34 days post i.a. injection. Imaging was performed in the near-infrared (NIR) 800nm fluorescence channel, corresponding to the emission wavelength of IR780. A fixed exposure time and gain setting

were used across all time points to ensure consistency in image acquisition. Fluorescence intensity was quantified using Image Studio Software (Li-Cor Biosciences). A region of interest (ROI) was manually defined around the knee joint to measure the total radiant efficiency. To correct for background fluorescence, an ROI was selected in a non-fluorescent region, and the signal was normalized accordingly.

2.6. Statistical analysis

For statistical analysis, GraphPad Prism 8.1.1 software (GraphPad Software, San Diego, CA, USA) was utilized. All data are expressed as the mean ± standard deviation (SD) of 3-5 independent repeated experiments, unless otherwise stated. Statistical significance was determined using a Student's *t*-test, unpaired, Mann-Whitney U test, and two-way analysis of variance (ANOVA). In all analyses, a *p*-value ≤ a is considered an indicator of statistical significance and is expressed as: * $p \leq 0.05$, ** $p \leq 0.01$, *** $p \leq 0.001$, **** $p \leq 0.0001$.

3. Results

3.1. Gelation time and injectability of P407-peptide hydrogel

P407 hydrogels exist in a fluid state below their critical gelation temperature (CGT), allowing them to flow and be easily injected. Upon increasing the temperature, these hydrogels undergo a sol–gel transition and form a semi-solid hydrogel (**Figure 1**). To assess the effect of polymer concentration on gelation behavior of hydrogel, varying concentrations of P407 (10, 15, 20, 25, and 30%) were prepared. Gelation times were recorded at room temperature (RT, 20 °C) and physiological temperature (37 °C) (**Table 1**). At concentrations of 10% and 15%, P407 hydrogels remained liquid at both RT and 37 °C, indicating that a minimum threshold of ≥18% is required for thermosensitive gelation, consistent with previous reports (26). Two-way ANOVA with multiple comparisons showed that increasing P407 concentration at both RT and 37 °C consistently increased the sol–gel transition temperature, with high statistical significance ($p \leq 0.0001$) (**Figure 1B**). Both 25% and 30% P407 formulations were selected for further evaluation owing to their favorable gelation profiles. In the next step, we validated the effect of of peptide incorporation on gelation behavior (1-7.5%) on 25 and 30% of P407. Addition of 1% self-assembling peptide to the 25% P407 formulation significantly reduced gelation times to 180 ± 9 s at RT and 32 ± 2 s at 37 °C compared with P407 alone ($p \leq 0.0001$ for both) (**Table 2**). Similarly, incorporation of 1% peptide into 30% P407 also shortened gelation times compared with 30% P407 alone (RT, $p = 0.002$; 37 °C, $p = 0.028$). However, increasing peptide concentrations (≥2%) in either 25% or 30% P407 formulations yielded highly viscous solutions with short gelation times at both RT and 37 °C. In the 25% P407 formulation, peptide concentrations ≥3% resulted in bulk gel formation (**Supplementary Figure 1**), while in the 30% P407 formulation, concentrations above 2% led to aggregation.

Since the goal was to identify the optimized hydrogel formulation based on gelation time at RT and 37 °C for subsequent intra-articular injection, injectability tests were performed on 25% and 30% P407 hydrogels containing 1% peptide using different needle gauges (**Figure 1C**). Both 25% and 30% P407 + peptide hydrogels could be injected relatively easy with no force through larger needles (18G and 23G). However, with smaller needle sizes (25G and 30G), the 30% formulation exhibited clogging and required relatively excessive force, particularly at 37 °C, which is unsuitable for intra-articular delivery (**Figure 1D**). By contrast, the 25% P407 + 1% peptide formulation could be injected smoothly through a 30G needle (used for animal experiments), without clogging or loss of control. Taken together, incorporation of 1% peptide into 25% P407 accelerated $T_{sol–gel}$ transition (RT: 223 ± 11 s vs. 180 ± 9 s, $p \leq 0.0001$; 37 °C: 44 ± 3 s vs. 32 ± 2 s, $p \leq 0.0001$) while maintaining injectability through a 30G needle, making it the optimized formulation for subsequent experiments, with 25% P407 alone used in parallel as control.

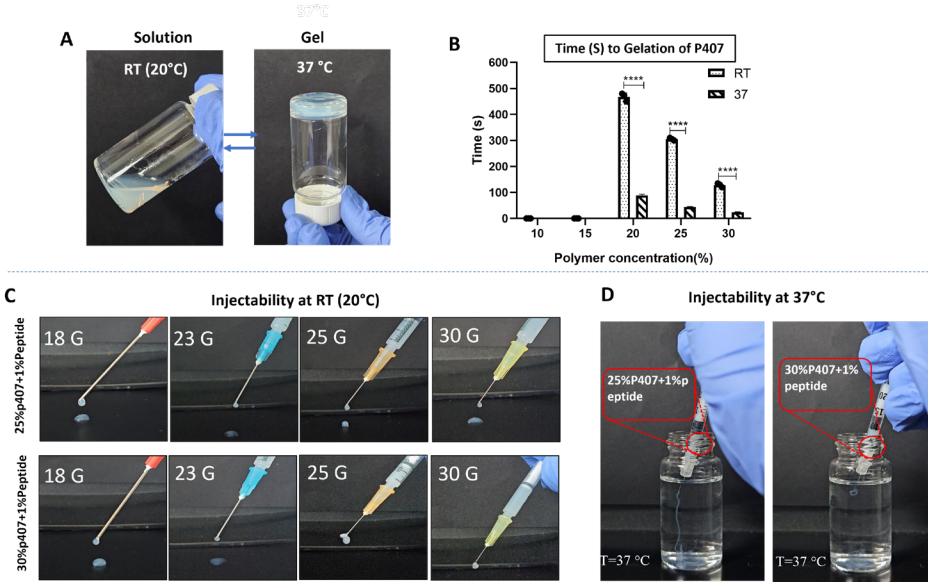

Figure 1. Gelation behavior and injectability of P407 and P407–self-assembling peptide hydrogels. (A) Representation of sol–gel transition of 25% P407 hydrogel by test tube inversion method **(B)** Quantitative analysis of gelation times at RT (20 °C) and 37 °C, showing significantly reduced gelation times upon peptide incorporation.**(C)** Injectability test of hydrogel composition of 1% self-assembling peptide into 25% and 30% P407 through different needle gauges (18G, 23G, 25G, 30G) at RT (20 °C). **(D)** Injectability assessment of 25% and 30% of P407 with 1% peptide throw needle 30G at 37°C. Statistical significance was determined using two-way ANOVA with multiple comparisons, with *p*-values indicated as *$p \leq 0.05$, **$p \leq 0.01$, ***$p \leq 0.001$, and ****$p \leq 0.0001$.

Table 1. Gelation time of P407 at various polymer concentrations.

Formulation	Time (s) to gelation at RT (20°C)	Time (s) to gelation at 37°C
10% P407	-	-
15% P407	-	-
20% P407	467±16	90±4
25% P407	305±5	44±2
30% P407	125 ±8	24±2

Reported in seconds measured at room temperature (RT) and at 37° C. Results are shown as means of a triplicate measurement ± standard deviation (SD).

Table 2. Gelation time of 25% P407 and 30%P407 in corporation with various self-assembling peptide

Formulation	Time (s) to gelation at RT (20°C)	Time (s) to gelation at 37°C
25% P407 + 1%Peptide	180±9	32±2*
25% P407 + 2%Peptide	45±4	9±1
25% P407 + 3%Peptide	32±4	7±1
25% P407 + 4%Peptide	16±3	Bulk
25% P407 + 5%Peptide	Bulk	Bulk
25% P407 + 7.5%Peptide	Bulk	Bulk
30% P407+ 1%Peptide	110±13	18±2
30% P407+ 2%Peptide	30±2	Bulk
30% P407+ 3%Peptide	Bulk	Bulk
30% P407+ 4%Peptide	Bulk	Bulk
30% P407+ 5%Peptide	Bulk	Bulk
30% P407+ 7.5%Peptide	Bulk	Bulk

Reported in seconds measured at room temperature (RT) and at 37 °C. Results are shown as means of a triplicate measurement ± standard deviation (SD). * Chosen for subsequent experiment.

3.2. Rheology characterization of the hydrogel

Rheological studies were conducted to assess the gelation kinetics and stiffness of 25% (w/v) P407 control and the same concentration of P407-peptide hydrogel formulations. First, gels were fully formed at 37°C and then subjected to an oscillation amplitude at a constant frequency, where the G' and G'' were measured when the strain increased exponentially. As visualised in **supplementary Figure 2**, both hydrogels show a sharp decline in gel strength above a strain of 0.6%. An appropriate strain before the breaking point of the gel (0.1 %) was chosen for subsequent experiments. Next, the gelation kinetics upon heating and cooling of gel formulations were assessed. Herein, the gelation temperature (Tgel) is defined as the temperature at which G' overtakes G''. Both formulations displayed a progressive rise of the G' from Tgel to 37 °C (**Figure 2A and B**), which can be attributed to the thermosensitive nature of the poloxamer-based polymer. In particular, P407 control showed a Tgel of 23.0 °C, while the addition of the self-assembling peptide decreased the Tgel to 20.5 °C, as summarised in **Table 3.** Furthermore, at 37 °C, the P407-peptide hydrogel exhibited a higher G' of 18.1 kPa compared to 16.6 kPa for the P407 control, reflecting improved stiffness. These enhancements in mechanical properties are evident from the progressive increase in G' during the heating cycle and support the utility of the P407-peptide hydrogel as a robust and thermosensitive platform for sustained drug delivery applications.

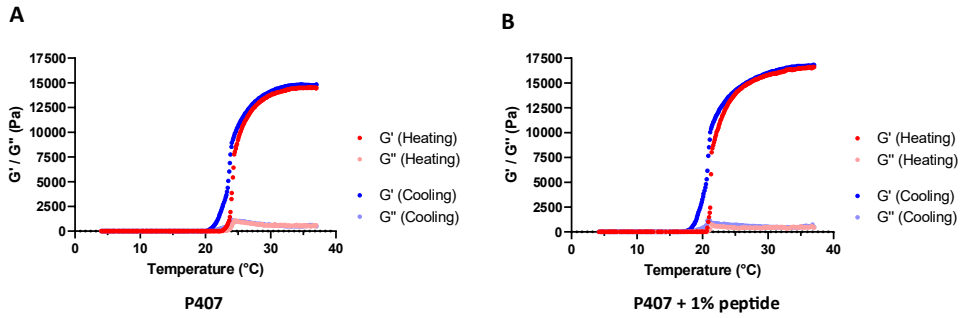

Figure 2: Average gelation profile of (A) P407 control and (B) P407 with 1 % self-assembling peptide gel formulations. Graphs depict the G' and G'' upon heating and cooling the samples between 4 and 37 °C, with each point representing the average of n = 3 measurements.

Table 3: Gelation temperature of 25% P407 control and 25%P407- peptide hydrogel formulation.

Formulation	T at G' > G'' (Heating, **)	T at G' < G'' (Cooling, **)	Maximum G' (kPa, *)
25% P407	23.0 ± 1°C	20 ± 1°C	16.6 ± 0.67
25% P407-peptide	20.5 ± 0.1°C	17 ± 1°C	18 ± 0.13

Each measurement was performed in triplicate. Statistical significance was determined using *t* test where significance results shown as * $p \leq 0.05$) or ** ($p \leq 0.01$).

3.3. Morphology of 25% P407 and 25% P407-peptide

SEM revealed that 25% P407 and the corresponding P407-peptide hydrogels revealed the typical porous structure of lyophilized P407 hydrogel specimens (**Figure 3**). Pores were predominantly round and oval, with pore sizes ranging from 40 ± 8.6 µm for 25% P407 and 92 ± 17.88 µm for 25% P407-peptide as analyzed by ImageJ software. The porous morphology corresponds to the P407 micelle-based network formed during gelation, which is dependent on polymer concentration.

Dynamic light scattering (DLS) analysis (**Supplementary Figure 3**) confirmed micelle formation at 1% P407. At this concentration, the average micelle size was 6.5 ± 0.38 nm for 1% P407 and 136.1 ± 10.59 nm for 1% P407-peptide. Increasing polymer concentration led to a corresponding increase in average particle size in both hydrogel types, likely due to micelle aggregation and closer packing at higher concentrations and elevated temperatures. This effect was more pronounced in the P407-peptide formulation. The larger particle size observed in the peptide-containing hydrogel correlated with the formation of a more open and expanded porous network, as confirmed by SEM.

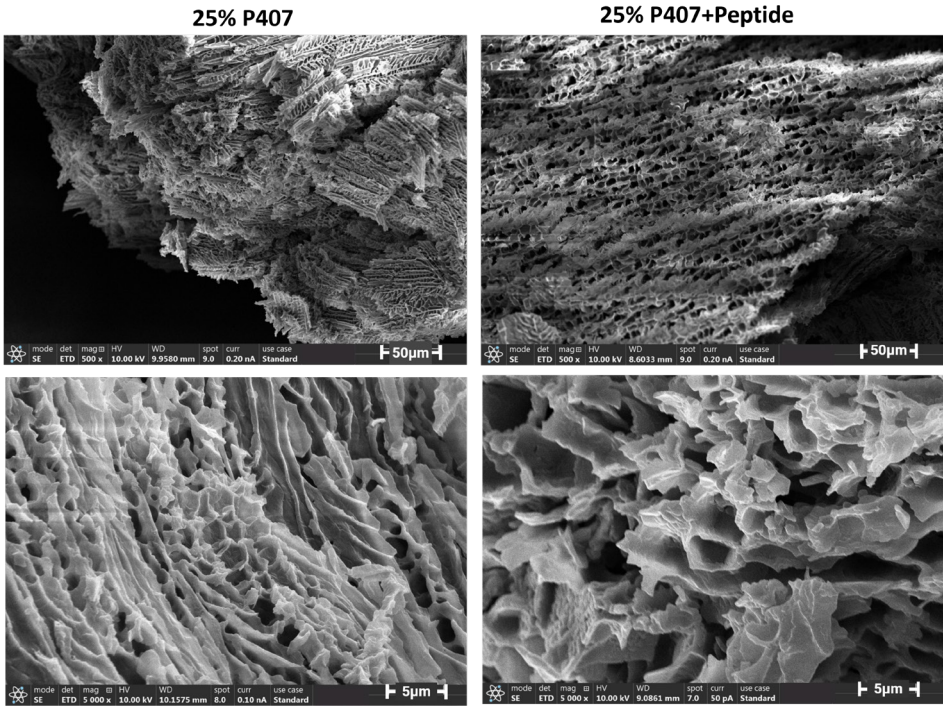

Figure 3: SEM images showing cross-sections of the 25% P407 and 25% P407 containing 1% self-assembling peptide hydrogels. Representative images are shown at 50 nm and 5 nm magnifications.

3.4. 25% (w/v) P407-self-assembling peptide hydrogel enhances hydrogel stability in aqueous solutions

The stability of the 25% (w/v) P407–self-assembling peptide hydrogel was evaluated in comparison with 25% P407 alone by analyzing hydrogel degradation and the release kinetics of IR780 over time. Data were analyzed using two-way ANOVA. In the degradation profiles (**Figure 4A**), both hydrogels showed progressive degradation over time. However, the P407 formulation showed a marked acceleration in degradation. Initially, at the first five time points (≥ 12 h), there was no significant difference in gel mass between the two formulations. However, at 24 h, the mass of the remaining gel was significantly higher in the P407 + peptide formulation (77 ± 3%) compared to P407 alone (60 ± 2%, $p = 0.036$). This difference became more pronounced at later time points; by 72 h, only 33 ± 2% of the P407 hydrogel remained, while 57 ± 4% of the P407 + peptide hydrogel was still intact ($p \leq 0.0001$). At 168 h (Day 7), the P407 hydrogel was entirely degraded (6 ± 1%), whereas the P407 + peptide hydrogel retained 13 ± 2% of its original mass and remained intact until day 9 (216 h).

To further investigate the impact of peptide incorporation on release kinetics, the cumulative release of IR780 from 25% P407 and 25% P407 + 1% peptide hydrogels was monitored over 216 h (**Figure 4B**). During the initial 24 h, approximately 65% of the initially loaded IR780 was released from both hydrogels. However, after 48 h, the release rate from the P407-peptide hydrogel significantly decreased compared to the P407 alone ($p \leq 0.05$ to ***$p \leq 0.0001$). Specifically, at 48 h, P407 released 80 ± 4% of the dye, compared to 73 ± 4% from P407 + peptide ($p = 0.014$). At 72 h, the release from P407 reached 83.8 ± 4%, while P407 + peptide released 75.2 ± 4% ($p = 0.008$). By day 7 (168 h), P407 was fully degraded, resulting in complete dye release, whereas the P407 + peptide formulation retained approximately 11% of the dye, indicating enhanced release control and a more sustained release profile. These findings align with the slower degradation observed in peptide-modified hydrogels, underscoring the stabilizing effect of peptide incorporation.

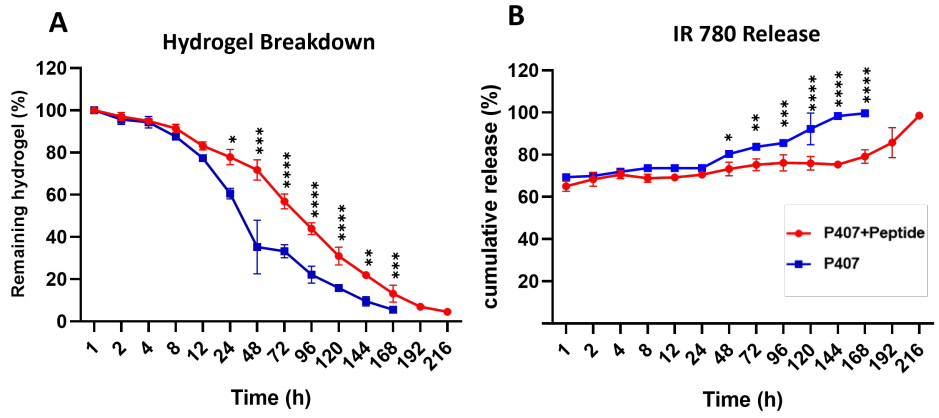

Figure 4: Hydrogel breakdown and IR780 Release Profile of 25% P407 and P407-Peptide hydrogels. (A) Degradation profiles of hydrogels monitored over time. **(B)** Cumulative release of IR780 dye from hydrogels over 216 h. Data are presented as mean ± SD (n = 3) and analyzed using two-way ANOVA. Statistical significance is indicated as $p \leq 0.05$, $p \leq 0.01$, $p \leq 0.001$, $p \leq 0.0001$.

3.4. Cell viability

The cytocompatibility of the 25% (w/v) P407 with and without self-assembling peptide hydrogel was assessed in human chondrocyte (C28/I2) cells using the MTS assay and LIVE/DEAD staining.

Based on statistical quantification using two-way ANOVA, and as shown in **Figure 5A**, the viability of untreated cells as well as cells exposed to 25% P407 and 25% P407 + peptide hydrogels was significantly higher compared to the cytotoxicity control (50% DMSO). The percentage of viable cells in the untreated, exposed to 25% P407, and 25% P407 + peptide groups remained high at all time points (24, 48, and 72 h), with no significant differences among these groups overall. However, cells treated with 25% P407 hydrogel alone exhibited lower viability than those treated with P407 + peptide at 24 h and 72 h ($p \leq 0.05$). These findings indicate that both hydrogels are non-cytotoxic, with the peptide-modified hydrogel demonstrating greater compatibility with C28/I2 cells.

The viability of the cells treated with 25% P407 + peptide hydrogel was further evaluated by LIVE/DEAD staining Live-dead assay after culturing for 1, 3 and 7 days (**Figure 5B-C**). A relatively large proportion of viable cells (green fluorescence) could be seen at all time points, while only a few dead cells (red fluorescence) were found (**Figure 5C**). Quantitative analysis of live/dead cell counts confirmed this observation (**Figure 5B**). Two-way ANOVA revealed a significantly higher number of viable cells compared to dead cells at day 1 ($p = 0.0154$), day 3 ($p = 0.0336$), and day 7 ($p = 0.0002$). Furthermore, a progressive increase in live cell density was noted from day 1 to day 7, indicating that the hydrogel supported not only cell survival but also proliferation. Specifically, the live cell population increased significantly from day 1 to day 3 ($p = 0.0009$) and from day 3 to day 7 ($p = 0.0020$).

These results demonstrate the excellent cytocompatibility of the 25% (w/v) P407–self-assembling peptide hydrogel, supporting its further evaluation for i.a. drug delivery applications.

3.5. *In vivo* degradation study

The *in vivo* degradation behaviour and retention capacity of the thermosensitive injectable hydrogel was assessed by direct 30-gauge needle injection of IR780-laden 25% (w/v) P407 or P407–peptide hydrogels into the right knee joints of DMM mice. PBS free IR780 was used as a control. Each formulation was comprised of 50 ng IR780. The intensity of fluorescence was measured at different sampling time points with the PEARL imaging system (**Figure 6A**). The NIRF imaging of the injected knees up to 34 days (**Figure 6B**) further verified that all formulations were properly delivered into the joint cavity as indicated by strong initial fluorescence signals within the joint cavity. In the PBS group, fluorescence intensity declined rapidly, becoming faint by day 14 and nearly undetectable by day 21. On the other hand, clearance from the P407 +1% peptide hydrogel group was relatively slow, and fluorescence was observed even on day 28 post- injection with residual signals remaining on day 34. This demonstrates that the presence of peptides greatly prolongs the retention time of hydrogel *in vivo*. Qualitative observations were supported by the quantitative analysis (**Figure 6C**).

Two-way ANOVAs showed that fluorescence intensities of both P407 and P407/peptide-based gels were significantly higher than PBS at all tested time points post-surgery ($p \leq 0.05$). Furthermore, P407/peptide hydrogel had statistically higher signal retention than the P407 alone at days 1, 7, 14

and 21 ($p \leq 0.05$). However, after 28 days the changes between groups were no longer statistically significant suggesting a general decrease of signal in all conditions.

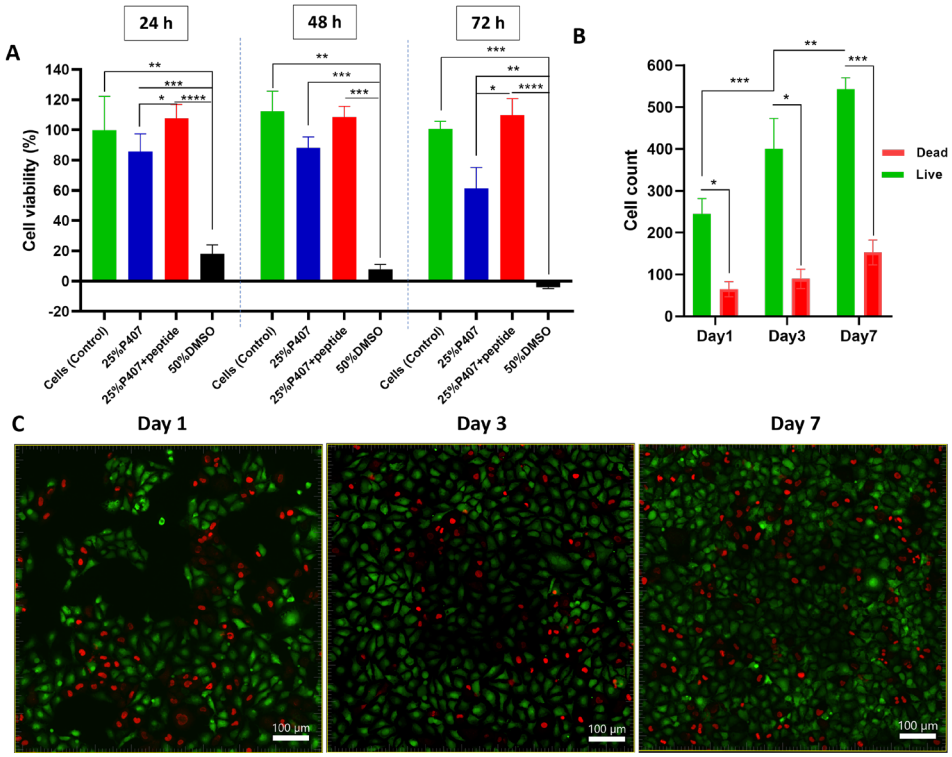

Figure 5: Evaluation of C28/I2 cell viability exposed to hydrogel using MTS assay. **(A)** MTS assay of C28/I2 cells incubated for 24, 48, and 72 h with 25% P407 or 25% P407 + peptide hydrogels. Cells cultured without hydrogel served as negative controls, while 50% DMSO was used as a positive cytotoxicity control. **(B)** Quantification of the number of live and dead cells based on LIVE/DEAD assay after 1, 3, and 7 days of culture. **(C)** LIVE/DEAD® staining of chondrocytes seeded on 25% P407- peptide hydrogels after 1, 3 and 7 days in culture. Live cells are stained green (calcein-AM), and dead cells are stained red (ethidium homodimer-1). Statistical analysis was performed using two-way ANOVA with multiple comparisons; significance levels are indicated as *$p \leq 0.05$, **$p \leq 0.01$, ***$p \leq 0.001$, and ****$p \leq 0.0001$. Scale bar = 100 µm.

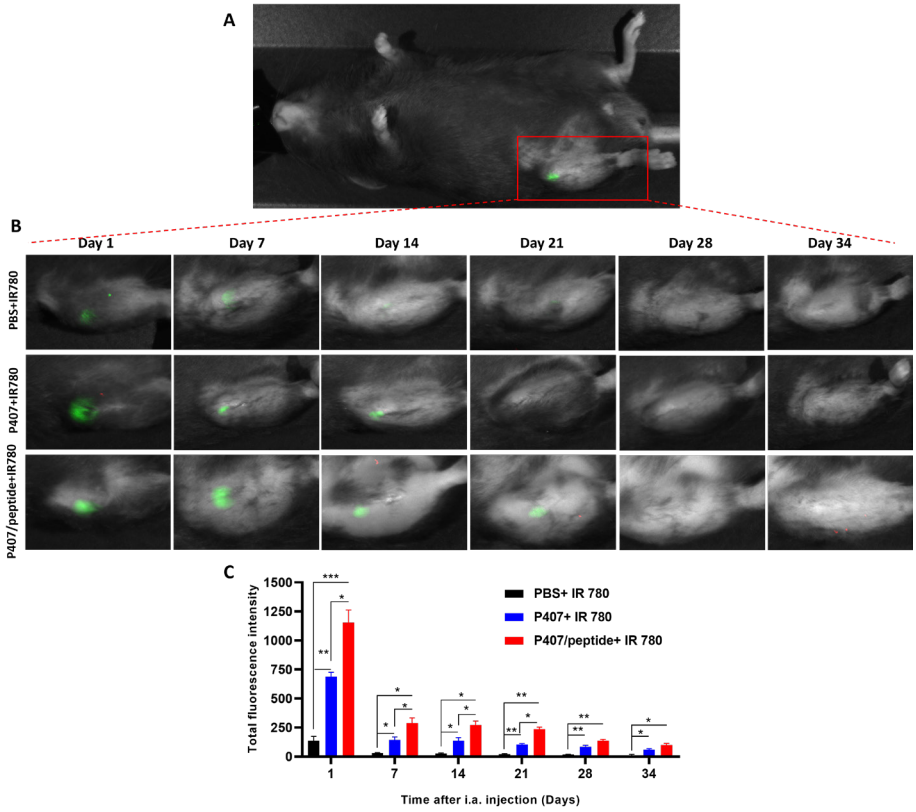

Figure 6. *In vivo* near-infrared fluorescence (NIRF) imaging and quantitative analysis of i.a injected formulations in the mouse model. **(A)** Setup of mice in the Pearl imaging system for NIRF acquisition. **(B)** Representative NIRF images of IR780 fluorescence in the right knee joints of mice treated with PBS + IR780,P407 + IR780, or P407-self-assembling peptide + IR780, captured on days 1, 7, 14, 21, 28, and 34 post-injection. **(C)** Quantification of total fluorescence intensity over time. Data are presented as mean ± SD (n = 6). Statistical analysis was performed using two-way ANOVA followed by appropriate multiple comparisons testing. Statistical significance was determined by appropriate tests and is indicated as *$p \leq 0.05$, **$p \leq 0.01$, and ***$p \leq 0.001$. i.a.= Intra.articular

4. Discussion

In this study, we formulated and characterized a thermosensitive injectable hydrogel composed of 25% (w/v) P407 and 1% (w/v) of a self-assembling peptide (Palmitoyl-WKGNNQQNYQQ). The formulations were designed to optimize intra-articular applications of therapeutic entities i.e. enhancing stability of the P407 hydrogel in an aqueous solutions while still benefitting from its thermos-sensitive properties. Our results showed that the optimal formulation of 25% P407 containing 1% peptide achieved an excellent balance of injectability and gelation, remaining fluid at

room temperature for handling while rapidly forming a gel at 37 °C. Moreover, SEM imaging confirmed a more porous microstructure in the peptide-containing hydrogel compared with P407 alone, consistent with supramolecular co-assembly between peptide nanofibers and P407 micelles. Degradation and release studies demonstrated that peptide incorporation slowed P407 dissolution and enabled more controlled, sustained release compared with P407 alone, linking release behavior to the enhanced stability of the hydrogel.. *In vitro* studies showed that the 25% P407 + 1% peptide hydrogel demonstrated good cytocompatibility with C28/I2 chondrocytes, maintaining high viability and attachment comparable to controls. The improved degradation and stability profiles were further confirmed *in vivo* using i.a injections in mouse knee joints. The P407–peptide hydrogel showed partial and gradual degradation, consistent with the slower dissolution observed *in vitro*. Together incorporation of 1% of our peptide to 25% of P407 appeared to reach an optimal formulation that remained fluid at room temperature for ease of handling and rapidly gel at body temperature to prevent undesired drug dispersion following injection (27, 28).

Our *in vitro* degradation studies revealed that our peptide-enhanced formulation remained intact for 9 days, reflecting increased stability of P407 with self-assembling peptide in aqueous environments. This prolonged stability is particularly beneficial for intra-articular drug delivery, where extended hydrogel presence supports sustained release and tissue interaction. The slower degradation observed in the P407 with self-assembling hydrogel is likely attributable to stabilizing molecular interactions between the peptide nanofibers and P407, including hydrogen bonding and hydrophobic associations that reduce water penetration and delay matrix erosion.

Based on the fact that we previously showed that the Palmitoyl-WKGNNQQNYQQ peptides in deionized water, formed stable β-sheet structures, while exposure to electrolyte solutions triggered self-assembly into nanofibrous networks (21, 29, 30). Moreover, due to the fact that the peptide sequence itself is amphiphilic, with tryptophan (W) and tyrosine (Y) contributing hydrophobic aromatic domains and polar groups, lysine (K) providing positive charge, asparagine (N) and glutamine (Q) offering polarity, and glycine (G) serving as a flexible connector networks are being formed. In addition, the palmitoyl tail is highly hydrophobic, driving amphiphilic self-assembly. Likewise, P407 is an amphiphilic block copolymer composed of hydrophobic PPO and hydrophilic PEO units that form micelles in aqueous solution. When combined, the amphiphilic peptide and P407 micelles co-assemble through hydrophobic insertion, hydrogen bonding, and other non-covalent interactions, resulting in a reinforced hydrogel network with larger pores. This organization, further stabilized by peptide-driven β-sheet nanofiber formation, accounts for the observed accelerated gelation, increased mechanical integrity, and prolonged stability of the peptide-modified hydrogel. These supramolecular interactions not only explain the larger pore size observed in SEM images of P407 and peptide and the delayed degradation but also justify the rationale for incorporating the peptide into P407 to enhance structural stability while preserving its thermosensitive properties. The stabilizing effects observed in our peptide-modified P407 hydrogel are consistent with previous reports where amphiphilic peptides were combined with P407 to reinforce its micellar network. Dzyhovskyi et al. demonstrated that P407 micelles form a three-dimensional network capable of physically entrapping amphiphilic Palmitoyl-GHK peptides, where the hydrophobic palmitoyl tail inserts into PPO domains and the peptide sequence interacts with the aqueous environment. This dual localization slowed peptide release, increased formulation stability, and generated a mechanically more robust gel than

peptide solution alone (31) Similarly, Gradinaru et al. reported that the aromatic dipeptide amphiphile Fmoc-FF interacts with P407 micelles, co-assembling into a hybrid supramolecular network with enhanced mechanical properties and tunable gelation dynamics (32) These studies, together with our findings, highlight the capacity of self-assembling peptides to interpenetrate the micellar domains of P407 and generate hybrid supramolecular structures with superior stability. On a different note there has been many studies in which P407 has been combined with extracellular matrix (ECM)-like components such as glycosaminoglycans and/ or HA to force thermosensitive properties upon these biomimetic EMC-materials (33, 34). Nonetheless, these high-MW polysaccharides are notoriously difficult to combine with P407 because dissolution of the P407 occurs rapidly through water-mediated erosion resulting in rapid clearance times while higher concentration of these high-MW polysaccharides increase room temperature viscosity and complicate small gauge injection. (35, 36). Together, the fact that our 1% amphiphilic peptide easily co-assembles with amphiphilic P407 micelles, enables strengthening of the network without affecting workable 30 G injectability, further highlights the strength of using such peptides rather than ECM-like components to mitigate innate limitations related to P407.

To comply to ethical and efficiency of animal experimentation, the *in vivo* characterization of the 25% P407 + 1% peptide hydrogel formulation was part of larger preclinical studies in which the therapeutic efficacy of extracellular vesicles (37) and a small pharmaceutical compound (38) was tested in a osteoarthritis DMM mouse model [REF to DMM model]. Using osteoarthritic instead of healthy knees could be considered a weakness of our study. On the other hand, the 25% P407 + 1% hydrogel was successfully used as carrier for intra-articular application of these therapeutic entities. Moreover, as outlined in both these studies P407 + peptide supported sustained release, without any local infection-histological or immunohistochemical reactive behavior.

In conclusion, our findings show that adding a self-assembling peptide to a poloxamer-based thermosensitive hydrogel that demonstrated favorable injectability, rapid gelation, and sustained release behavior. The formulation was cytocompatible and showed promise as an intra-articular delivery platform. While the study did not include *in vivo* mechanical testing, detailed chemical characterization, or GMP-scale validation, these aspects represent natural next steps toward translation rather than undermining the current findings. Taken together, our results provide a strong preclinical foundation supporting further optimization and evaluation of this hydrogel–peptide system as a versatile carrier for regenerative and disease-modifying therapies in OA.

Acknowledgments

The research leading to these results has received funding from the European Union's Horizon 2020 research and innovation program AutoCRAT under grant agreement No 874671. The material presented and views expressed here are the responsibility of the author(s) only. The EU Commission takes no responsibility for any use made of the information set out.

Author Contributions

S.S.S and L.J.C designed the experiments. S.S.S., S.M.L., and S.R. performed the *in vitro* experiments. S.S.S. and T.S. performed the *in vivo* experiments. S.S.S. was responsible for most of the data and statistical analysis and drafting of the manuscript. All authors have read, revised and agreed to the published version of the manuscript.

References

1. Li J, Mooney DJ. Designing hydrogels for controlled drug delivery. Nature Reviews Materials. 2016;1(12):1-17.

2. Liu Y, Yin P, Chen J, Cui B, Zhang C, Wu F. Conducting polymer-based composite materials for therapeutic implantations: from advanced drug delivery system to minimally invasive electronics. International Journal of Polymer Science. 2020;2020:1-16.

3. Raucci MG, D'Amora U, Ronca A, Ambrosio L. Injectable functional biomaterials for minimally invasive surgery. Advanced healthcare materials. 2020;9(13):2000349.

4. van de Looij SM, de Jong OG, Vermonden T, Lorenowicz MJ. Injectable hydrogels for sustained delivery of extracellular vesicles in cartilage regeneration. J Control Release. 2023;355:685-708.

5. Maudens P, Jordan O, Allemann E. Recent advances in intra-articular drug delivery systems for osteoarthritis therapy. Drug Discov Today. 2018;23(10):1761-75.

6. Huang H, Qi X, Chen Y, Wu Z. Thermo-sensitive hydrogels for delivering biotherapeutic molecules: A review. Saudi Pharm J. 2019;27(7):990-9.

7. Zhu C, Han S, Zeng X, Zhu C, Pu Y, Sun Y. Multifunctional thermo-sensitive hydrogel for modulating the microenvironment in Osteoarthritis by polarizing macrophages and scavenging RONS. J Nanobiotechnology. 2022;20(1):221.

8. Collett J, Weller P. Poloxamer Handbook of Phamaceutical Excipents Editor Kibbe. A. American Pharmaceutical Association, Washington DC and Royal Pharmaceutical Society, London, UK. host publication2000.

9. Yang RS, Chen M, Yang XX, Sun WZ, Lu C, Hui Q, et al. Modified poloxamer 407 and hyaluronic acid thermosensitive hydrogel-encapsulated keratinocyte growth factor 2 improves knee osteoarthritis in rats. Materials & Design. 2021;210:110086.

10. Akash MS, Rehman K. Recent progress in biomedical applications of Pluronic (PF127): Pharmaceutical perspectives. J Control Release. 2015;209:120-38.

11. Ludwig A. The use of mucoadhesive polymers in ocular drug delivery. Advanced drug delivery reviews. 2005;57(11):1595-639.

12. Boonlai W, Tantishaiyakul V, Hirun N, Sangfai T, Suknuntha K. Thermosensitive poloxamer 407/poly (acrylic acid) hydrogels with potential application as injectable drug delivery system. AAPS PharmSciTech. 2018;19(5):2103-17.

13. Ur-Rehman T, Tavelin S, Gröbner G. Chitosan in situ gelation for improved drug loading and retention in poloxamer 407 gels. International journal of pharmaceutics. 2011;409(1-2):19-29.

14. Wu H, Wang K, Wang H, Chen F, Huang W, Chen Y, et al. Novel self-assembled tacrolimus nanoparticles cross-linking thermosensitive hydrogels for local rheumatoid arthritis therapy. Colloids and Surfaces B: Biointerfaces. 2017;149:97-104.

15. Akkari AC, Papini JZB, Garcia GK, Franco MKD, Cavalcanti LP, Gasperini A, et al. Poloxamer 407/188 binary thermosensitive hydrogels as delivery systems for infiltrative local anesthesia: Physico-chemical characterization and pharmacological evaluation. Materials Science and Engineering: C. 2016;68:299-307.

16. Pereira GG, Dimer FA, Guterres SS, Kechinski CP, Granada JE, Cardozo NSM. Formulation and characterization of poloxamer 407®: Thermoreversible gel containing polymeric microparticles and hyaluronic acid. Química Nova. 2013;36:1121-5.

17. Dumortier G, Grossiord JL, Agnely F, Chaumeil JC. A review of poloxamer 407 pharmaceutical and pharmacological characteristics. Pharmaceutical research. 2006;23:2709-28.

18. Li Y, Qin M, Cao Y, Wang W. Designing the mechanical properties of peptide-based supramolecular hydrogels for biomedical applications. SCIENCE CHINA Physics, Mechanics & Astronomy. 2014;57(5):849-58.

19. Li Y, Cao J, Han S, Liang Y, Zhang T, Zhao H, et al. ECM based injectable thermo-sensitive hydrogel on the recovery of injured cartilage induced by osteoarthritis. Artif Cells Nanomed Biotechnol. 2018;46(sup2):152-60.

20. Balbirnie M, Grothe R, Eisenberg DS. An amyloid-forming peptide from the yeast prion Sup35 reveals a dehydrated beta-sheet structure for amyloid. Proc Natl Acad Sci U S A. 2001;98(5):2375-80.

21. Mas-Moruno C, Cascales L, Cruz LJ, Mora P, Pérez-Payá E, Albericio F. Nanostructure Formation Enhances the Activity of LPS-Neutralizing Peptides. ChemMedChem: Chemistry Enabling Drug Discovery. 2008;3(11):1748-55.

22. Bodratti AM, Alexandridis P. Formulation of Poloxamers for Drug Delivery. J Funct Biomater. 2018;9(1):11.

23. Chi SC, Jun HW. Release rates of ketoprofen from poloxamer gels in a membraneless diffusion cell. J Pharm Sci. 1991;80(3):280-3.

24. Wang Y, Nguyen DT, Yang G, Anesi J, Chai Z, Charchar F, et al. An improved 3-(4, 5-dimethylthiazol-2-yl)-5-(3-carboxymethoxyphenyl)-2-(4-sulfophenyl)-2H-tetrazolium proliferation assay to overcome the interference of hydralazine. ASSAY and Drug Development Technologies. 2020;18(8):379-84.

25. Glasson S, Blanchet T, Morris E. The surgical destabilization of the medial meniscus (DMM) model of osteoarthritis in the 129/SvEv mouse. Osteoarthritis and cartilage. 2007;15(9):1061-9.

26. Ur-Rehman T, Tavelin S, Grobner G. Chitosan in situ gelation for improved drug loading and retention in poloxamer 407 gels. Int J Pharm. 2011;409(1-2):19-29.

27. Rizzo F, Kehr NS. Recent Advances in Injectable Hydrogels for Controlled and Local Drug Delivery. Adv Healthc Mater. 2021;10(1):e2001341.

28. De Bardi M, Muller R, Grunzweig C, Mannes D, Boillat P, Rigollet M, et al. On the needle clogging of staked-in-needle pre-filled syringes: Mechanism of liquid entering the needle and solidification process. Eur J Pharm Biopharm. 2018;128:272-81.

29. Holmes TC, de Lacalle S, Su X, Liu G, Rich A, Zhang S. Extensive neurite outgrowth and active synapse formation on self-assembling peptide scaffolds. Proceedings of the National Academy of Sciences. 2000;97(12):6728-33.

30. Wang Y, Zhao L, Hantash BM. Support of human adipose-derived mesenchymal stem cell multipotency by a poloxamer-octapeptide hybrid hydrogel. Biomaterials. 2010;31(19):5122-30.

31. Dzyhovskyi V, Santamaria F, Marzola E, Montesi L, Donelli I, Manfredini S, et al. Production and Characterization of Semi-Solid Formulations for the Delivery of the Cosmetic Peptide Palmitoyl-GHK. Cosmetics. 2025;12(2):50.

32. Gradinaru VR, Bercea M, Gradinaru LM, Puiu A, Lupu A, Petre BA. Targeting Injectable Hydrogels: The Role of Diphenylalanine Peptide Derivative in the Gelation Dynamics of Pluronic® F127. Polymers. 2025;17(7):930.

33. Wenjie Fang FY, Wenhua Li , , Hu Q, , Chen W, , et al. Dexamethasone microspheres and celecoxib microcrystals loaded into injectable gels for enhanced knee osteoarthritis therapy. International Journal of Pharmaceutics. 2022;622.

34. Yu C, Li L, Liang D, Wu A, Dong Q, Jia S, et al. Glycosaminoglycan-based injectable hydrogels with multi-functions in the alleviation of osteoarthritis. Carbohydrate Polymers. 2022;290:119492.

35. Chen I-C, Su C-Y, Chen P-Y, Hoang TC, Tsou Y-S, Fang H-W. Investigation and characterization of factors affecting rheological properties of poloxamer-based thermo-sensitive hydrogel. Polymers. 2022;14(24):5353.

36. Abdeltawab H, Svirskis D, Hill AG, Sharma M. Increasing the Hydrophobic Component of Poloxamers and the Inclusion of Salt Extend the Release of Bupivacaine from Injectable In Situ Gels, While Common Polymer Additives Have Little Effect. Gels. 2022;8(8):484.

37. Sayedipour S, Nikkels J, Tertel T, ED Suchiman H, Balbi M, Shaw G, et al. Therapeutic efficacy of hiMSC-derived Extracellular Vesicles from Serum-containing and Xeno-free media for osteoarthritis treatment. bioRxiv. 2025:2025.08. 20.671255.

38. Sana Sayedipour S, Mazzini G, Tuerlings M, Nikkels J, Koedam M, Cruz LJ, et al. Evaluating the Therapeutic Efficacy of Iopanoic Acid in a DMM-Induced Osteoarthritis Mouse Model and Osteochondral Lesioned Human Explants. bioRxiv. 2025:2025.07. 15.663868.

Supplementary materials

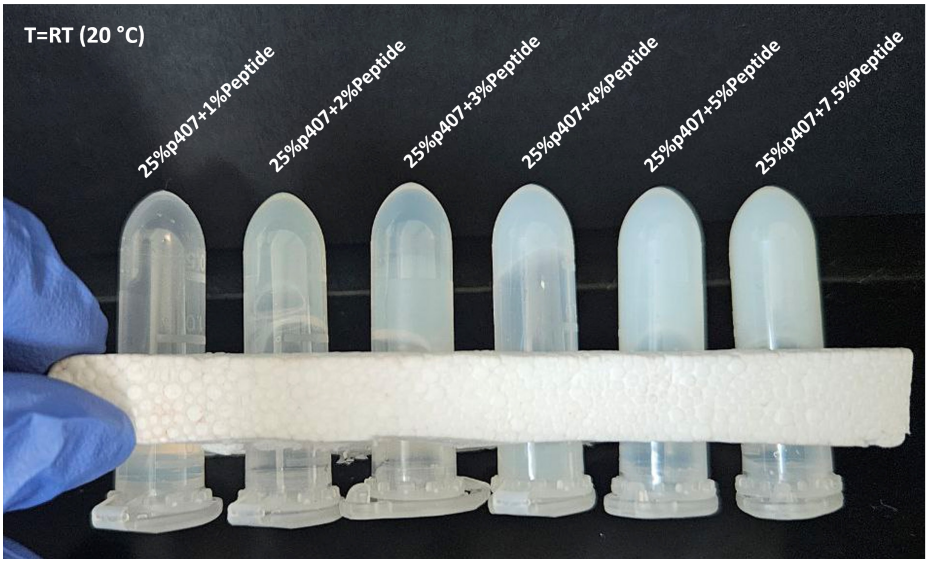

Supplementary Figure S1. Sol–gel transition of homogeneous mixtures of 25% (w/v) P407 hydrogel incorporating increasing concentrations of the self-assembling peptide (1%, 2%, 3%, 4%, 5%, and 7.5% w/v). The gelation behavior was assessed using the tube inversion method at room temperature (RT, 20 °C). Increasing peptide concentration resulted in a progressively more solid-like hydrogel appearance, indicating enhanced gel stability and faster gelation kinetics.

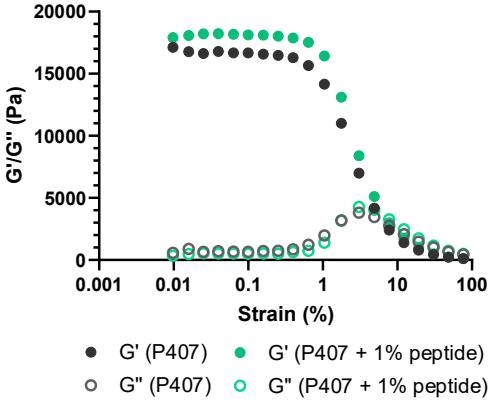

Supplementary Figure 2: Strain sweep of 25% P407 and 25% P407 -peptide hydrogels. G’ and G’’ were measured as strain was increased from 0.01% to 100% at a constant frequency of 1 Hz. A linear viscoelastic regime was observed for the strain range between 0.01% and 0.4%.

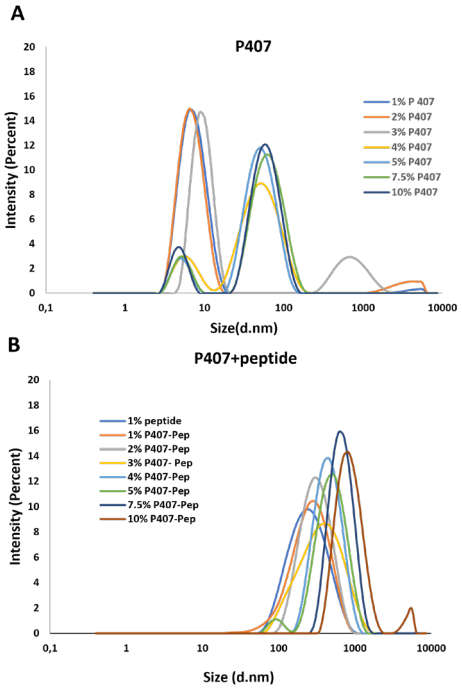

C DLS measurement of different folmulations of P407 and P4 peptide

Formulation	Size (d.nm)	PdI
1% P407	6.5 ± 0.38	0.199 ± 0.03
2% P407	7.38 ± 0.75	0.267 ± 0.04
3% P407	15.63 ± 4.53	0.489 ± 0.11
4% P407	22.63 ± 3.12	0.55 ± 0.14
5% P407	40.85 ± 1.23	0.606 ± 0.06
7.5% P407	32.34 ± 2.89	0.535 ± 0.05
10% P407	34.08 ± 6.64	0.607 ± 0.13
1% peptide	159.3 ± 25.8	0.255 ± 0.05
1%P407+Pep	136.1 ± 10.6	0.247 ± 0.01
2%P407+Pep	253.8 ± 11.7	0.218 ± 0.02
3%P407+Pep	301.8 ± 3.26	0.248 ± 0.016
4%P407+Pep	380.4 ± 13.9	0.227 ± 0.02
5%P407+Pep	412.2 ± 15.4	0.226 ± 0.01
7.5% P407+Pep	550.2 ± 22.1	0.236 ± 0.04

Supplementary Figure 3: DLS measurements with representative histogram with the pick size distribution and PdI valus for **(A)** 1, 2, 3, 4, 5, 7.5 and 10% (w/w) P407. **(B)** 1% peptide and P407-peptide. **(C)** summary table of average size and PdI values of different P407 and P407 + peptide formulations. All measurements were performed in triplicate. DLS = dynamic light scattering; PdI = polydispersity index.